Bioorganic Chemistry 87 (2019) 31–42

Contents lists available at ScienceDirect

Bioorganic Chemistry

journal homepage: www.elsevier.com/locate/bioorg

Cucurbitane-type compounds from *Momordica charantia*: Isolation, *in vitro* antidiabetic, anti-inflammatory activities and *in silico* modeling approaches

Siddanagouda R. Shivanagoudra[a], Wilmer H. Perera[a], Jose L. Perez[a], Giridhar Athrey[b], Yuxiang Sun[c], G.K. Jayaprakasha[a,*], Bhimanagouda S. Patil[a,*]

[a] Vegetable and Fruit Improvement Center, Department of Horticultural Sciences, Texas A&M University, 1500 Research Parkway, Suite A120, College Station, TX 77845, United States
[b] Department of Poultry Science, Texas A&M University, College Station, TX 77845, United States
[c] Department of Nutrition and Food Sciences, Texas A&M University, College Station, TX 77843, United States

ARTICLE INFO

Keywords:
Bitter melon
Cucurbitaceae
Triterpene aglycones
Murine macrophages
Molecular docking

ABSTRACT

Momordica charantia L., commonly known as bitter melon, belongs to the Cucurbitaceae family. Various *in vitro* and *in vivo* studies have indicated that extracts of bitter melons have anti-diabetic properties. However, very little is known about the specific purified compounds responsible for these antidiabetic properties. In the present study, 3β,7β,25-trihydroxycucurbita-5,23(E)-dien-19-al, charantal, charantoside XI, and 25ξ-isopropenylchole-5, 6-ene-3-O-D-glucopyranoside were isolated from bitter melon fruit. The structures of the purified compounds were elucidated by HR-ESIMS, 1D, and 2D NMR experiments. All compounds exhibited significant inhibition of α-amylase and α-glucosidase comparable to acarbose. Molecular docking studies demonstrated that purified compounds were able to bind to the active sites of proteins. Additionally, the purified compounds showed significant anti-inflammatory activity, downregulating the expression of *NF-κB, iNOS, IL-6, IL-1β, TNF-α,* and *Cox-2* in lipopolysaccharide-activated macrophage RAW 264.7 cells. Our findings suggest that the purified compounds have potential anti-diabetic and anti-inflammatory activities and therefore hold promise for the development of plant-based management for diabetic and inflammatory conditions.

1. Introduction

Diabetes is a chronic metabolic disease, and its frequency has been rapidly increasing worldwide in recent years [1]. The incidence of type II diabetes is predicted to grow by 6% annually. Current estimates report that by 2025, India, China, and the United States of America will have the highest number of people with diabetes [2]. Diabetes is a chronic disease that has a complex etiology, with hallmark pathology of hyperglycemia [3]. Several strategies have been used for managing the disease. However, certain drugs have adverse effects. Several synthetic drugs, including sulfonylureas (promoting insulin secretion), biguanides and thiazolidinediones (enhancing insulin utilization), acarbose and voglibose (inhibiting α-amylase and α-glucosidase) have been used to manage post-prandial hyperglycemia [1,3]. These synthetic drugs cause several side effects such as abdominal distention, diarrhea, nausea, and meteorism [4]. Despite significant developments over the last decade in treating Type II diabetes, many diabetic patients are unable to reach their recommended therapeutic targets. Therefore, it is necessary to develop safe and active natural anti-diabetic compounds that have less adverse effects than existing synthetic medications [5]. As a folk medicine, bitter melon is widely studied with regards to its antidiabetic effect and all parts of the plant have shown hypoglycemic activity. Bitter melon is a vegetable with high nutrition value, and its extracts have been reported to inhibit the activities of α-amylase and α-glucosidase enzymes, but the bioactive component remains elusive.

Bitter melon (*Momordica charantia* L.) is cultivated as a vegetable for the management of diabetes in tropical and subtropical areas such as East Africa, Asia, South America, and the Caribbean [6,7]. Among various health benefits, the anti-diabetic activity of bitter melon has been related to various triterpenoids. To date, more than 230 bitter melon cucurbitane triterpenoids have been reported from different plant parts including leaves, stems, roots, fruits, and vines [8–10]. Isolated cucurbitane triterpenoids and their glycosides have been reported to have significant anticancer [11] and antitumor activity [12], glucose reducing effect [13], and AMP-activated protein kinase activities [14]. In response to accumulating data correlating bitter melon and successful diabetes management, several preclinical and clinical trials have been conducted. Over 20 clinical studies have hypothesized

* Corresponding authors.
E-mail addresses: gkjp@tamu.edu (G.K. Jayaprakasha), b-patil@tamu.edu (B.S. Patil).

https://doi.org/10.1016/j.bioorg.2019.02.040
Received 2 January 2019; Received in revised form 16 February 2019; Accepted 18 February 2019
Available online 26 February 2019
0045-2068/

that extracts and bioactive compounds present in the bitter melon may be responsible for hypoglycemic activity [15,16].

Inflammation is an underlying cause of many chronic diseases such as diabetes mellitus and cardiovascular diseases [17]. Subclinical chronic inflammation is a common pathology in diabetes associated with changes of inflammatory biomarkers [18]. The release of pro-inflammatory cytokines, such as *IL-1β*, *IL-6*, *TNF-α*, other inflammatory mediators like nitric oxide (NO), prostaglandins (PGE_2), and the resulting activation of macrophages have significant effects on the development of diabetic complication [19]. The increased expression of inflammatory cytokines can amplify the inflammatory responses, leading to aggravation of diabetes and its long term complications including insulin resistance, neurodegenerative disorders such as Alzheimer's disease [20]. Recently, a few studies have explored the effect of bitter melon on inflammation, but the identification of the bioactive compounds responsible for this activity remains elusive [21,22].

The present paper describes the isolation and structural elucidation of four compounds from Chinese bitter melon fruit. Identified compounds were evaluated for the α-amylase and α-glucosidase inhibitory activities. Moreover, molecular docking study allowed us to determine the potential interactions of these compounds with the enzymes. Additionally, these compounds were investigated for anti-inflammatory properties using lipopolysaccharide (LPS)-activated RAW 264.7 macrophage cells.

2. Results and discussion

2.1. Structural elucidation of compounds

The ethyl acetate extract from Chinese bitter melon fruit was subjected to silica gel and reversed-phase flash chromatography to separate one new cucurbitane-type triterpene (compound **3**) together with two known triterpene aglycones (compounds **1** and **2**), and one sterol glucoside (compound **4**). Compounds **1, 2,** and **4** were characterized by 1D and 2D NMR and high-resolution mass spectroscopic data (Table 1 and Fig. S1). On the basis spectral data, compounds **1** and **2** were identified as 3β,7β,25-trihydroxycucurbita-5, 23(E)-dien-19-al (TCD) and charantal, respectively. The chemical shifts of these compounds were matched to reported data [23,24]. Previously, TCD and charantal were isolated from leaf extracts of *M. charantia*, and this is the first report of their isolation from edible fruit. Compound **4** was identified as 25ξ-isopropenylchole-5,(6)-ene-3-*O*-*β*-D-glucopyranoside (IDG), which was previously isolated from *M. charantia* [25].

Compound **3** was purified as a white amorphous powder, $[\alpha]_D^{25}$ −24.16 (*c* 0.1, MeOH). A HPLC chromatogram and UV spectra of compound **3** show the typical cucurbitane-type compound at around 220 nm (Fig. S2A and S2B). The Fig. S2C and S2D shows HR-TOF-ESIMS and HR-TOF-APCI of compound **3** with a molecular ion at *m/z* 523.34381 $[M+Na]^+$ and 523.3067 $[M+Na]^+$ (calculated *m/z* 523.3399 $[M+Na]^+$) respectively, suggesting a molecular formula of $C_{31}H_{48}O_5Na$. Eight compounds molecular weight matched to compound **3** with our published paper [10] and in-house database of all triterpenes and sterols isolated from *M. charantia* until 2018. However, none of these compounds NMR spectra matched to compound **3**. The ^{13}C Attached Proton Test (APT) NMR data of compound **3** (Fig. 1, Y-axis) showed 31 carbons with six methines (including one oxymethine group), seven methylenes, seven methyl groups, five quaternary carbons, one aldehyde, one carboxylic acid, and four olefinic carbons, one tri-substituted and three di-substituted. The complete assignments of HMQC correlations are shown in Fig. S3 and chemical shifts were presented in Table S1. The lack of olefinic carbons in kuguacin C, the presence of two tri-substituted olefinic carbons, and the absence of methoxy groups in the purified compound **3** suggested its structural novelty. Further, the side chain of compound **3** was identified through HMBC and DQF-COSY. The side chain chemical shifts of compound **1** were compared with kuguacin A and S, and momordicine VII [23,26,27]. Also, NMR signals of rings A-D of compound **3** were also similar to those reported for compound **1**. The main difference was found in a signal that appeared at 168.3 ppm, assigned as a carbonyl of a carboxylic acid due to confirmed molecular weight obtained from HR-MS data. The ^3J HMBC correlation of 168.3 ppm with 4.82 ppm together with important HMBC correlations of the A ring and COSY correlations, corroborated the position of the carboxylic acid (Fig. 2). Complete assigned 1D and DQF-COSY data for compound **3** are shown in Figs. S4–S7. On the basis of the above spectral data, compound **3** was named as charantoside XI. The structures of identified compounds **1–4** were shown in Fig. 2.

2.2. Inhibition of α-amylase and α-glucosidase activity

The inhibitory effect of purified compounds on α-amylase and α-glucosidase at two concentrations were tested and results were compared with acarbose (Fig. 3A). Compounds **1–4** showed inhibition of 44–61% and 63–79% of α-amylase at 0.43 mM and 0.87 mM concentrations respectively. Acarbose exhibited significantly higher inhibitory activity (88%) at 0.13 mM. Among the isolated compounds, IDG showed the highest inhibitory activity (79%) followed by charantal (70%) and TCD (69%) against α-amylase at 0.87 mM concentration. The novel compound, charantoside XI, showed moderate inhibition of 62% against α-amylase.

Similarly, inhibition of α-glucosidase was evaluated at 0.67 mM and 1.33 mM concentrations and results were compared with positive control acarbose at 0.06 and 0.13 mM (Fig. 3B). Maximum of 81.9% inhibition was observed for acarbose at 0.13 mM, followed by IDG (71%), TCD (65%), charantal (60%) and charantoside XI (56%) at 1.33 mM. The inhibitory activity of compounds **1–4** may be due to their differences in structural configuration. Nevertheless, TCD has been demonstrated for reducing the blood glucose level in diabetes-induced male ddY mice and showed moderate anti-HIV activity with EC_{50} value of 25.62 μg/mL [26,28]. In the present study, TCD showed good inhibitory activity against the two enzymes. In addition, IDG showed significantly higher inhibition compared to the other compounds and comparable activity to that of acarbose. The suppression of salivary pancreatic α-amylase and α-glucosidase in the brush border membrane of small intestine regulates the digestion of complex carbohydrates, which in turn controls the blood glucose [29]. The inhibitory mechanism of these compounds may be due to conformational changes derived from the presence of a sugar moiety in IDG, possibly allowing the binding of IDG to these enzymes. A higher number of attachments of sugar moieties would be needed to further evaluate the influence of cucurbitane glycosides on the inhibition of these enzymes.

2.3. Molecular docking

2.3.1. Virtual molecular docking study for inhibition of α-amylase by the purified compounds

In order to predict the mode of interactions of compounds **1–4** with α-amylase, molecular docking was carried out using Autodock 4.2. The enzyme α-amylase is composed of A, B, and C domains. Domain A is the largest with residues 1–99 and 169–404. Domain A forms a central eight-stranded parallel β-barrel with active site residues Asp197, Glu233, and Asp300. Domain B is the smallest (residues 100–168) and forms a calcium binding site against the wall of the β-barrel of domain A. Protein groups making ligand interactions with this calcium include Asn100, Arg158, Asp167, and His201. Domain C (residues 405–496) is made up of an antiparallel β-structure and is loosely associated with domains A and B [30]. The refined α-amylase structure is well characterized and has a network of water molecules occupying the cleft of the active site and hydrogen-bonding with polar side chains of Asp300, Glu233, and Aspl97, with the chloride ligand Asn298, and with the main chain through Ala307 N and Trp59 [31]. Also, the binding cleft is characterized by aromatic residues such as Trp58, Trp59, Tyr62,

Table 1
^{1}H and ^{13}C NMR data for purified compounds **1**, **2**, and **4** from the EtOAc extract of *Momordica charantia*.

	Compound 1 ($CDCl_3$)		Compound 2 (CD_3OD)		Compound 4 (pyridine-d_5)	
Position	δH (ppm)	δC (ppm)	δH (ppm)	δC (ppm)	δH (ppm)	δC (ppm)
1	1.76; 1.54	21.4	1.31, m; 1.21, m	35.8	1.00, m; 1.77, m	37.66
2	1.95; 1.90	28.6	1.82, m; 1.31, m	28.7	2.12, m; 2.18, m	30.27
3	3.55 (1H, m)	76.3	3.46 br, s	77.2	3.99, m	78.84
4	–	41.6	–	42.4	2.49, m; 2.77, m	39.46
5	–	145.7	–	147.5	–	140.84
6	5.88 (1H, br d, *J* = 3.9 Hz)	124.2	5.81 (1H, dd, *J* = 1.7, 5.3 Hz)	124	5.37 (br s)	122.2
7	3.95 (1H, br d, *J* = 4.7 Hz)	66.5	3.92 (d, *J* = 5.2 Hz)	67	1.90, m; 1.95, m	32.36
8	2.07 m	47.8	2.45 (1H, m)	37.8	1.4, m	32.23
9	–	50.1	1.83	51	0.92, m	50.36
10	2.51 (1H, br dd *J* = 12.0; 4.0 Hz)	36.8	–	46.7	–	37.1
11	2.21; 1.57 m	23.8	1.53, m; 1.40, m	22.3	1.38, m; 1.48, m	21.47
12	1.93; 1.39 m	27.6	1.79, m; 1.66, m	29.7	1.12, m; 2.02, m	39.98
13	–	45.5	–	45.3	–	42.5
14	–	47.8	–	51.4	1.01, m	56.86
15	1.37; 1.37 m	34.9	1.36, m; 1.32, m	23.4	1.55, m; 1.55, m	24.67
16	1.68; 1.68 m	29.2	1.66, m; 1.56, m	29.96	1.30, m; 1.84, m	28.65
17	1.49 m	50.1	1.45 (1H, m)	51.2	1.06, m	56.28
18	0.87 (3H, s)	15.1	0.81 (3H, s)	15.5	0.69 (3H, s)	12.15
19	9.71 (1H, s)	208.5	0.71 (3H, s)	18.9	0.95 (3H, s)	19.61
20	1.49	36.4	1.45 (1H, m)	37.7	1.44, m	35.94
21	0.89 (3H, s)	18.9	0.84 (3H, d, *J* = 5.8 Hz)	19.3	0.88 (3H, d, *J* = 6.3 Hz)	19.1
22	2.12; 1.71	39.3	2.05; 1.71 (2H, m,m)	40.4	1.07, m; 1.41, m	34.15
23	5.57 (1H, m)	125.3	5.48 (1H, m)	126		30.45
24	5.55 (1H, d, *J* = 14.4 Hz)	139.9	5.48 (1H, d, *J* = 6.34 Hz)	141	1.27, m; 1.83, m	29.83
25	–	70.9	–	71.4	1.94, m	49.85
26	1.29 (3H, s)	30.2	1.16 (3H, s)	29.98	1.39, m; 1.39, m	26.95
27	1.29 (3H, s)	30.1	1.16 (3H, s)	29.87	0.87 (3H, t, *J* = 7.8 Hz)	12.51
28	1.04 (3H, s)	27.4	0.98 (3H, s)	27.9	–	147.81
29	1.23 (3H, s)	25.6	1.15 (3H, s)	26.3	4.83, m; 4.90, m	112.21
30	0.73 (3H, s)	18.1	9.78 (1H, s)	210.1	1.64 (3H, s)	18.01
Glu-1′					5.06 (d, *J* = 7.3 Hz)	102.69
Glu-2′					3.99, m	75.47
Glu-3′					4.3 (dd, *J* = 6.7, 7.9 Hz)	78.75
Glu-4′					4.31, m	71.4
Glu-5′					–	78.26
Glu-6′					4.32 (dd, *J* = 2.2, 11.7 Hz); 4.48 (dd, *J* = 4.7, 11.5 Hz)	63.1

His101, Pro163, Ile235, Tyr258, His305, and Ala307 [31,32]. The three main residues Aspl97, Glu233, and Asp300 are close together in the active site of α-amylase and are known as the binding cleft, which lies in a deep depression at the center of α-amylase [33,34].

The results of the 3D molecular docking images of compounds **1–4** are shown in Fig. 4A–4D. The 2D schematic ligand-protein complex images are shown in Fig. S8. All compounds were anchored to the catalytic site of α-amylase through various bonds. Table 2 summarizes the binding affinity and binding interactions of purified compounds **1–4** with α-amylase (PDB ID: 1OSE). As shown in Fig. 4A, the refined docking of TCD generated the best docking pose with a minimum binding energy of −10.55 kcal/mol. The 2D schematic Fig. S8A and 3D diagram (Fig. 4A) illustrate TCD inserted into the cavity of α-amylase. TCD interacted with amino acid residues Glu233, Ile235, Lys200, Tyr151, Gly306, His305, Trp59, Trp58, Val163, and Leu162 in domain A of α-amylase. Five hydrogen bonds were found between TCD and amino acid residues (Glu233, Ile235, Tyr151, Gly306, and His305) with bond lengths of 4.02, 3.45, 6.84, 3.85, and 4.06 Å, respectively. These hydrogen bonds strengthened the interactions between TCD and α-amylase. The interactions of TCD also includes alkyl and pi-alkyl interactions between Trp59, Trp58, Val163, and Leu162.

Similarly, charantal was bound to the active site of α-amylase with binding energy −8.76 kcal/mol. Fig. 4B and Fig. S8B shows charantal interacted with crucial amino acid residues including Trp58, His305, Trp59, Val163, Leu162, Lys200, His201, Ile235, and Glu240 in domain A of α-amylase. Hydroxyl groups at position C-3 and C-25 of charantal formed strong conventional hydrogen bonds with amino acid residues Trp59 and Glu240 with a bond length of 4.47 and 4.81 Å, respectively. We also observed pi-alkyl and alkyl interactions of charantal with several amino acid residues including Trp58, His305, Val163, Leu162, Lys200, His201, and Ile235 with bond lengths of 5.30, 5.25, 5.14, 4.69, 4.35, 5.85, and 4.08 Å respectively.

The refined docking of charantoside XI with α-amylase generated the best docking pose with a minimum binding energy of −9.79 kcal/mol. The 3D schematic in Fig. 4C and Fig. S8C shows that charantoside XI established several hydrogen bonds within the α-amylase enzymatic pocket and interacted with several amino acid residues, including Glu233, Gly306, Trp59, Gln63, Trp58, His305, Val163, Leu162, and Ile235 (Fig. S8C). Four conventional hydrogen bonds were established between charantoside XI and the active pocket of α-amylase, in which the carboxylic acid at position 3 formed H-bonds with Trp59 and Gly63 with a bond length of 4.23 and 4.29 Å, respectively. Similarly, hydroxyl groups at C-25 and the CHO group at C-19 position established hydrogen bonding with Glu233 and Gly306 with a bond length 3.26 and 3.75 Å, respectively. Charantoside XI also established pi-alkyl and alkyl interactions with Ile235, Leu162, Val163, His 305, Trp58 with bond lengths of 4.69, 5.25, 5.76, and 5.78 Å, respectively.

Fig. 4D displays a 3-D schematic interaction of IDG with α-amylase. IDG generated the best docking pose with a minimum binding energy of −11.98 kcal/mol, which indicates that IDG showed the strongest binding affinity with the α-amylase protein. The strong binding affinity may be related to IDG's high α-amylase inhibitory activity observed in our study (78.9%). IDG was found to anchor at the catalytic site of α-amylase by making conventional hydrogen bonds to residues Gly306, Glu240, and Gly306 resulting in a potent inhibition of α-amylase.

It is interesting to notice that the minor difference of chemical structure between IDG and cucurbitane compounds **1–3** affected greatly in molecular docking results. The absence of two methyls at position 28,

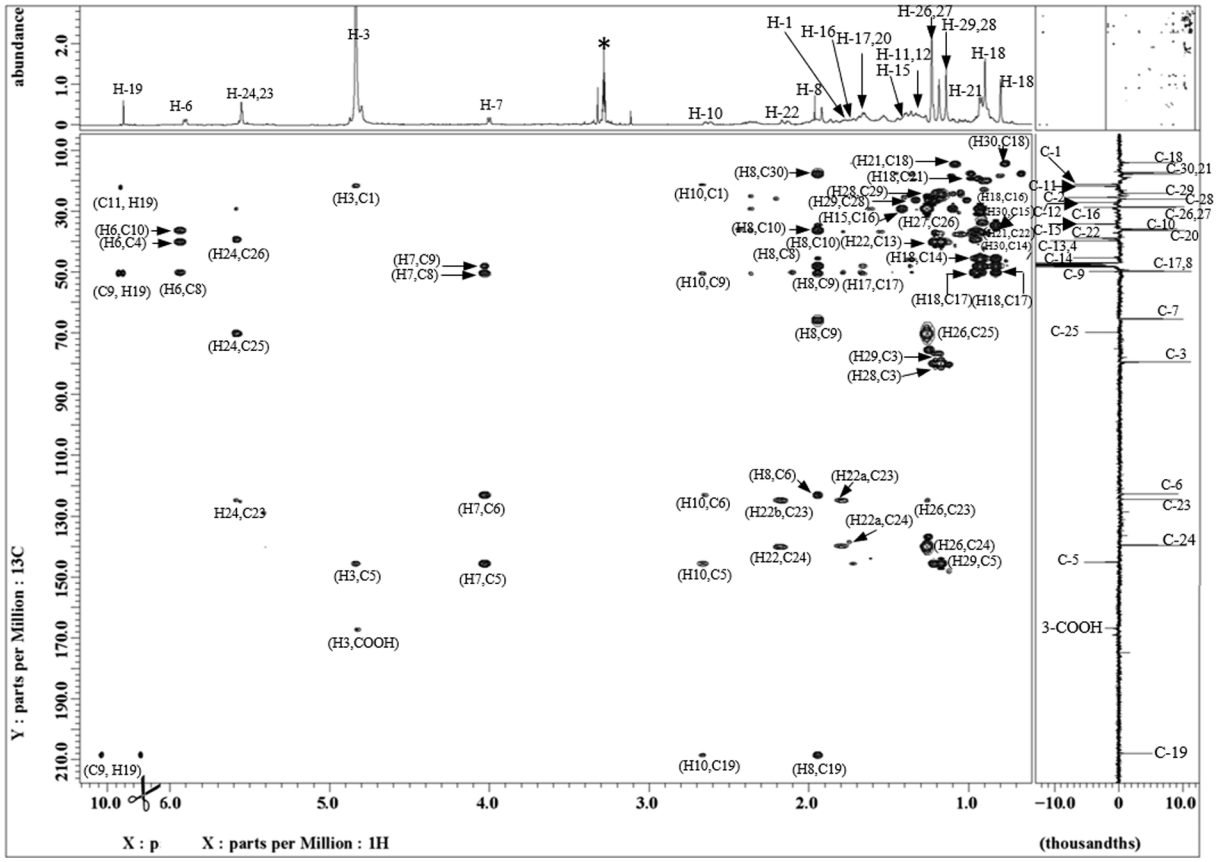

Fig. 1. Complete assignments of HMBC spectra of compound **3** (charantoside XI). Spectra were recorded in MeOH-d_4. ^{1}HNMR on X-axis and ^{13}C attached proton test (APT) is on the Y-axis of the spectrum. The solvent signal is marked with an asterisk (*).

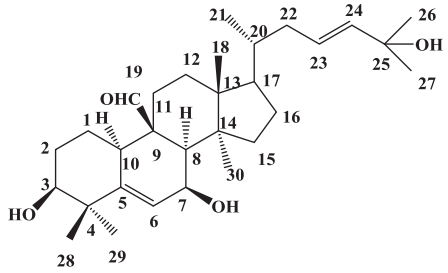

3β,7β,25-trihydroxycucurbita-5,23(E)-dien-19-al (1)

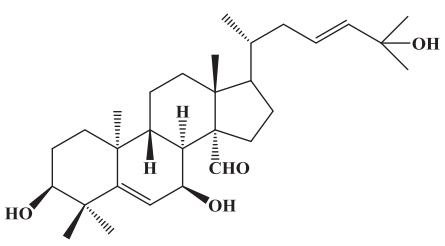

Charantal (2)

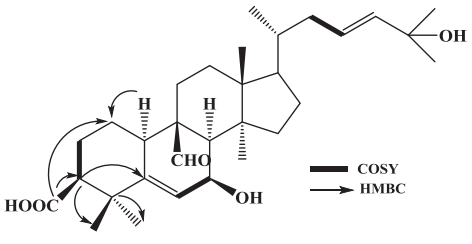

Charantoside XI (3)

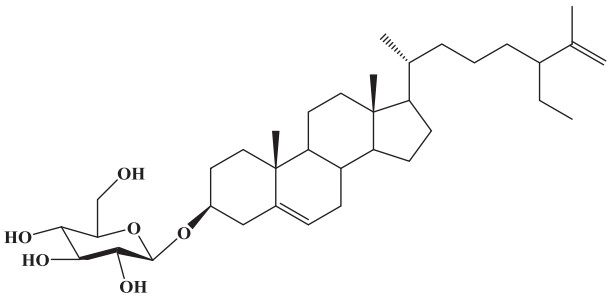

25ξ–isopropenylchole-5,(6)-ene-3-*O*-*β*–D-glucopyranoside (4)

Fig. 2. Structures of identified compounds (**1–4**) from the EtOAc extract of *M. charantia* and important COSY and HMBC correlations in compound **3**.

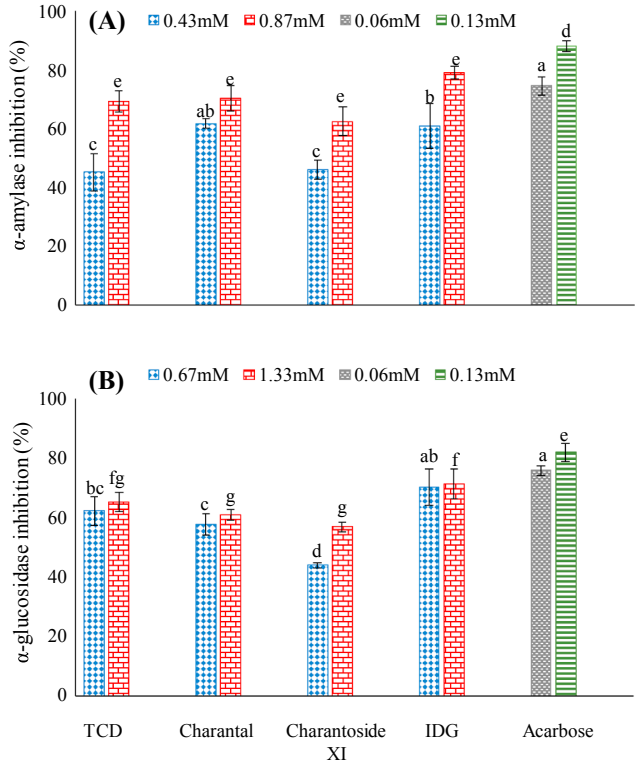

Fig. 3. Effect of purified compounds on the inhibition of (A). α-amylase and (B). α-glucosidase, acarbose was used as a positive control and all the experiments were conducted in triplicate with two biological replications. The results are represented as means ± SD for (n = 6). Identical letters at each concentration are not significantly different at $p \leq 0.001$. Abbreviations, TCD: (3β,7β,25-trihydroxycucurbita-5,23(E)-dien-19-al) and IDG: 25ξ-isopropenylchole-5,(6)-ene-3-O-β-D-glucopyranoside.

29 in A ring and attachment of glucose sugar moiety at position C-3 in IDG was more favorable for getting significantly lower binding energy of −11.98 kcal/mol compared other compounds. A lower binding energy means the ligand is more accessible to bind with the protein. Moreover, IDG showed the highest α-amylase inhibition activity among the four compounds. This may be due to the addition of monosaccharide to the structure affects the polarity of the compound and in turn, affects the bioactivity. Also, we observed altered docking pose for compound **3** due to the attachment of glucose moiety. However, the glucose moiety on position 3 of IDG was able to bind with the side chain of Glu240. Therefore, it is very important to note that, interactions between glucose on the A ring and protein residues were suspected to play an important role in determining the binding energy among compounds bearing the same backbone.

2.3.2. Virtual molecular docking study for inhibition of α-glucosidase by the purified compounds

To understand the interact action of α-glucosidase, molecular docking analysis was carried out to investigate the binding mode of compounds within the binding pocket of α-glucosidase. To date, the crystal structure of α-glucosidase from *Saccharomyces cerevisiae* (the enzyme used for the biological assay) has not been resolved [3]. Therefore, the compounds were docked to isomaltase crystal structure 3A4A downloaded from the Protein Data Bank. Isomaltase from *S. cerevisiae* co-crystallized with maltose has 85% similarity to yeast α-glucosidase (MAL12) through homology modeling [18]. Asp69, His112, Arg213, Asp215, Glu276, His351, Asp352, and Arg442 are key residues in the active catalytic site of α-glucosidase [35].

The binding energy of TCD, charantal, charantoside XI and IDG with interacting residues, including H-bond interacting residues and Van der Waals interacting residues, along with the number of H-bonds with the crystal structure of isomaltase from *S. cerevisiae* are presented in Table 2. The 3D schematic and 2D interactions of TCD are shown in Fig. 5A and Fig. S9A. TCD interacted with crucial amino acid residues, namely Lys156, Ser241, Ser240, Asp307, Arg315, Phe303, Arg442, His280, Asp242, and Tyr158. According to the Autodock 4.2 simulation results, the α-glucosidase–TCD inhibitor complex showed −10.87 kcal/mol binding energy. TCD made five hydrogen bonds with interacting residues Lys156, Ser241, and Asp305, and two hydrogen bonds with His208. The hydroxyl group at position 25 established two hydrogen bonds with Lys156 and Ser241 with bond lengths of 4.34 and 3.97 Å, respectively. Similarly, the hydroxyl group at position 7 of TCD established two hydrogen bonds with His280 with bond lengths of 4.26, 5.38 Å. The aldehyde group at position 19 was able to establish a hydrogen bond with Asp307 with a bond length of 5.74 Å. Moreover, the hydroxyl group at position 3 formed Van der Waals interaction with Arg442 with a bond length of 3.98 Å, which is key interaction to inhibit enzyme to a greater extent. Indeed, the docking analysis for the compounds from the previous study showed that compounds were surrounded by residues Glu277, His351 and Asp352, which are part of the catalytic residues of isomaltase [36].

Charantal had a binding energy of −10.78 kcal/mol and occupied the active region of isomaltase by interacting with amino acid residues Lys156, Phe303, Gly353, Glu411, Arg315, Tyr158, and Ser240. The 2D schematic (Fig. S9B) and 3D interactions of charantal are shown in Fig. 5B. In the conformation of isomaltase–charantal complex, the three hydroxyl groups at position 3, 7, and 25 of the ligand formed hydrogen bonds with the amino acid residues Lys156, Gln353, and Glu411 with bond lengths of 4.14, 4.53, and 4.61 Å, respectively. These hydrogen bonds overtly strengthened the interaction between charantal and isomaltase. Methyl and aldehyde groups at position 18 and 30 established robust Van der Waals bonding with amino acid residues Arg315 and Ser240 with bond lengths of 4.32 and 3.40 Å, respectively. The above interactions resulted in an inhibition constant of 12.91 nM.

The binding mode of charantoside XI in the active site of isomaltase was shown in Fig. 5C and Fig. S9C. The ligand was stabilized in the active site of an enzyme by interacting with amino acid residues Phe314, Leu313, Arg315, Phe159, As 69, Arg442, Tyr158, Phe303, and Phe314. The carboxylic acid group at position 3, hydroxyl groups at positions 7 and 25, and the aldehyde group at position 19 formed five conventional hydrogen bonds with Asp307, Leu313, Arg315, Asp69, and Arg442 with bond lengths of 5.10, 5.00, 5.48, 4.60, and 6.42 Å, respectively. The interaction between the ligand and the catalytic residue Arg442 was essential for the inhibition of isomaltase. The methyl groups at positions 18, 29, and 21 formed pi-alkyl interactions with amino acid residues Tyr58, Phe59, and Phe314. Finally, the binding energy was −10.4 kcal/mol, and the inhibition constant was 23.86 nM.

IDG was bound to residues Leu313, Asp242, Pro312, Val308, Val319, and His280 at the catalytic site of isomaltase. The 2D schematic and 3D interactions of IDG are shown in Fig. S9D and Fig. 5D. IDG generated the best docking pose with a minimum binding energy of −10.58 kcal/mol. The ligand was surrounded by catalytic residue Asp 242, and the interaction was likely crucial for inhibition of the isomaltase. Three conventional hydrogen bonds were formed in which C-2′ and C-3′ on the sugar moiety formed H-bonds with Leu313 (3.94 and 4.98 Å) and Asp242 (5.16 Å). These hydrogen bonds strengthened the interactions between IDG and isomaltase. IDG formed pi-alkyl and alkyl interactions between Val308, Val319, and His280 with bond lengths of 4.63, 4.46, and 5.31 Å, respectively.

2.4. Effect on inflammatory gene expression of macrophages

Four purified compounds **1–4** from bitter melon were tested for anti-inflammatory activity in LPS-activated RAW 264.7 macrophages. All of the compounds tested differentially affect the expression of *NF-κB, iNOS, IL-6, IL-1β,* and *Cox-2* with the exception of *TNF-α*, which was

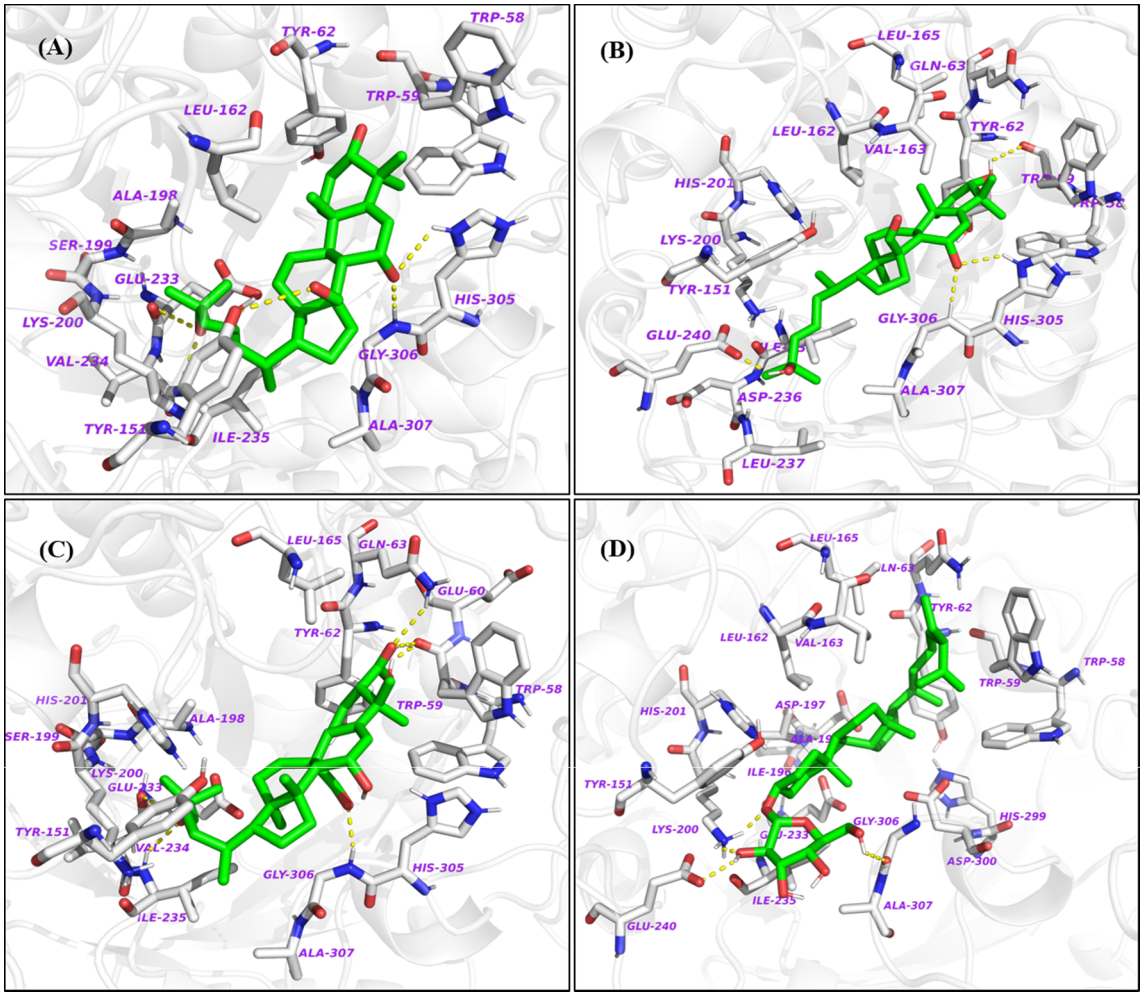

Fig. 4. The 3D ligand-protein interactions for (A). 3β,7β,25-trihydroxycucurbita-5,23(E)-dien-19-al, (B). charantal, (C). charantoside XI, and (D). 25ξ-isopropenylchole-5,(6)-ene-3-O-β-D-glucopyranoside, in the binding pocket of α-amylase. The ligands in the 3D structure are shown in green and hydrogen bonds are shown in yellow. (For interpretation of the references to colour in this figure legend, the reader is referred to the web version of this article.)

not significantly different from the LPS control group regardless of the treatment (Fig. 6). A significant decrease in the expression of *NF-κB*, *iNOS*, *IL-1β*, and *Cox-2* was observed in the TCD treatment group when compared to the LPS control group. Similar results were found in the cells treated with charantoside XI and IDG, with the exception of *NF-κB* displaying levels similar to the LPS control group. The expression of *iNOS, IL-1β*, and *Cox-2* was significantly lower compared to the LPS group, while the expression of NF-κB was not affected in the charantal treatment group. Surprisingly, the level of IL-6 dramatically increased in response to treatment of cells with charantal. TCD, charantal, and charantoside XI are structurally similar; however, they differ in the position of the aldehyde and carboxylic acid groups, which may be responsible for their anti-inflammatory activity. TCD and charantoside XI have an aldehyde group at position 19 and both significantly downregulated the expression of *NF-κB*, *iNOS*, *IL-1β*, *COX-2* compared to the LPS-treated control. Charantal has an aldehyde group at position 30, and it was not observed to be significantly different from the LPS-activated cells for *NF-κB* and *TNF-α*. In charantoside XI, the presence of a carboxylic acid group at position 3 showed significant suppression of pro-inflammatory cytokines *iNOS, IL-1β*, and *Cox-2*. The IDG phytosterol glucoside did not induce considerable suppression of pro-inflammatory cytokines *NF-κB*, *IL-6*, and *TNF-α*. However, IDG treatment did downregulate *iNOS*, *IL-1β* and *Cox-2* compared to the LPS control group. IDG has a glucose moiety in position 3, while the other tested compounds have a hydroxyl or carboxylic acid group in that position. It is widely accepted that slight variation in the chemical structures of bioactive compounds can influence its activity. Our results show that regardless of the similarities of the triterpenoid nucleus, slight structural differences affect the expression of genes involved in the regulation of the inflammatory response in RAW 264.7 macrophages.

Several triterpenoids have been isolated from various plants and evaluated for their bioactive potential [37,38]. The structure–function activities of this class of compounds fluctuate in response to modifications to the 3 position [39]. In this study, we observed that the glucose molecule attached to position 3 did not counteract the effect of LPS in inducing the expression of *NF-κB*, *IL-6*, and *TNF-α* and for the most part the effect of gene expression was not as pronounced at the other treatment compounds. Previous reports evaluating the bioactivity of triterpenoids have concluded that an increase in the number of glucose molecules or differences in its attached position may alter the compound's bioactivity by steric hindrance. Additionally, the change in the number and position of hydroxyl groups may alter its polarity and, in turn, its interaction with membrane phospholipids, resulting in altered bioactivities [40]. Therefore, it is crucial to elucidate the composition of bitter melon metabolites further to understand better how these compounds may be used as beneficial treatments for the management of diabetes and other inflammation-mediated diseases. While more in-depth studies are required for a definitive assessment of the anti-inflammatory properties of these compounds, this screening procedure is useful for possibly narrowing down potential targets for further studies.

Table 2
Binding affinity and binding interactions of purified compound (**1–4**) with porcine pancreatic α-amylase (PDB ID: 1OSE) and α-glucosidase (PDB ID: 3A4A).

Receptor	Compound	Binding energy (kcal/mol)	Hydrogen bonds	Interactions	Hydrogen bonds	Inhibition constant (nM)
α-Amylase (PDB ID:1OSE)	TCD	−10.55	5	Glu233, Ile235, Tyr151, Gly306, His305, Trp59, Trp58, Val163, Leu162	Ile235 (3.45 Å), Glu233 (3.45 Å), Tyr151 (6.84 Å), Gly306 (3.85 Å), His305 (4.06 Å)	18.53
	Charantal	−8.76	2	Trp59, His305, Trp58, Ile235, Lys200, His201, Leu162, Val163, Tyr62	Glu240(4.81 Å), Trp59 (4.47 Å)	377.84
	Charantoside XI	−9.79	4	Glu233, Gly306, Gly63, Trp59, Gly306, His305, Val163, Leu162, Ile235	Glu233 (3.26 Å), Gly306 (3.75 Å), Trp59 (4.29 Å), Gly63 (4.23 Å)	66.39
	IDG	−11.98	4	Trp59, Trp58, His305, Tyr62, Leu162, Ala198, Gly306, Glu240 Lys200, Ile235, His201, Leu165, Val163	Glu240(4.81 Å), Trp59 (4.47 Å), Lys200 (5.82, 4.67 Å),	1.65
α-Glucosidase (PDB ID:3A4A)	TCD	−10.87	5	Lys156, Ser241, Asp307, Arg315, Phe303, Arg442, His280, Asp242, Tyr158	Lys156 (4.34 Å), Ser241 (3.97 Å), Asp197 (4.26 Å), His280 (5.38 and 5.74 Å)	10.68
	Charantal	−10.78	3	Ser240, Lys156, Phe303, Gly353, Glu411, Arg315, Tyr158, Ser240	Lys156 (4.14 Å), Glu411 (4.61 Å), Gly353 (4.53 Å)	12.48
	Charantoside XI	−10.4	4	Phe314, Leu313, Arg315, Phe159, Asp69, Arg442, Tyr158, Phe303, Phe314	Leu313 (5.10 Å), Asp307 (5.00 Å), Asp69 (4.60 Å), Arg442(6.42 Å)	23.86
	IDG	−10.58	3	Leu313, Asp242, Pro312, Val308, Val319, and His280	Leu313 (4.98 and 3.94 Å), Asp242 (5.16 Å)	12.23

For example, *NF-κB* is a major component of the signaling cascade that leads to an inflammatory response resulting in the production of inflammatory cytokines such as *iNOS*, *TNF-α*, and *IL-lβ*.

3. Conclusions

In this study, a new cucurbitane-type triterpene aglycone and other three compounds were isolated from the fruit of *M. charantia*. These compounds showed differential α-amylase and α-glucosidase inhibitory activities ranging from 56 to 79%. Molecular docking studies of both enzymes revealed that all four compounds predominantly occupied the active site of the proteins and H-bonds were formed between the enzyme and hydroxyl groups in the cucurbitane skeleton. In the α-amylase molecular docking study, purified compounds showed interactions with crucial amino acid residues including Glu233, Trp59 with binding energies between −8.76 and −11.98 kcal/mol and inhibition constants of 1.65–377 nM. Similarly, in the α-glucosidase molecular docking studies, compounds **1–3** showed interactions with crucial amino acid residue Arg442 and binding energies of −10.57 to −10.88 kcal/mol. Furthermore, the isolated compounds were screened for anti-inflammatory effect using RAW 264.7 macrophages. The results indicated that the purified compounds from bitter melon have the potential to act as anti-inflammatory agents by lowering the expression of inflammation-related markers. Therefore, bitter melon fruit might have potential therapeutic application in diabetic and inflammation-related conditions.

4. Experimental

4.1. Chemicals

Silica-gel 6 Å particle size (40–63 μm), glacial AcOH, phosphate-buffered saline (PBS), and RPMI-1640 were purchased from VWR International (Radnor, PA). The RAW 264.7 mouse monocyte-macrophage cell line was procured from the American Type Culture Collection (ATCC, USA). Fetal bovine serum (FBS), penicillin, streptomycin, *n*-hexane, $CHCl_3$, MeOH, ACN, $(CH_3)_2CO$, EtOAc, ACN drum grade, and MeOH (HPLC grade), D-(+)glucose, dinitrosalicylic acid (DNSA), dextrose, sodium chloride, acarbose, and Porcine Pancreatic α-amylase (PPA) were purchased from Sigma-Aldrich (St. Louis, MO). Genes including *GAPDH, Cox-2*, *TNF-α*, *IL-6*, *IL-1β*, *iNOS*, *NF-κB* and the Aurum Total RNA Mini Kit, iScript cDNA synthesis kit, and SsoAdvanced Universal SYBR Green Supermix were purchased from Bio-Rad Laboratories (Hercules, CA). Silica gel 60 F_{254} thin-layer chromatography plates, HCl, and H_3PO_4, were obtained from EMD Millipore, Burlington, MA). RP-C_{18} cosmosil 140 was obtained from Nacalai Tesque, Inc, (Kyoto, Japan). Flash silica gel cartridges (Redi*Sef* ®R_f) were procured from Teledyne ISCO, Lincoln, NE. Perdeuterated MeOH, $CHCl_3$, and pyridine were purchased from Cambridge Isotope Laboratories, Inc. (Tewksbury, MA, USA). Nano-pure water (18.2 MΩ-cm) was obtained from a NANO pure purification system (Barnstead/Thermolyne, Dubuque, IA).

4.2. General experimental procedure

Optical rotations were measured on a ATAGO SAC -i polarimeter in MeOH at 25 °C. The analysis of column fractions was performed using an Agilent 1200 Series HPLC (Agilent, Foster City, CA) system consisting of degasser, quaternary pump, autosampler, column oven, and a diode array detector. The separation was carried out using an RP C_{18} Gemini series column (250 × 4.6 mm; 5 μm) (Phenomenex, Torrence, CA), with a flow rate of 0.8 mL/min. The oven temperature was set at 40 °C and chromatograms were recorded at 210, 280, and 320 nm. The elution was carried out using gradient mode elution with 3 mM phosphoric acid (A) and acetonitrile (B). Initially, elution was carried out in isocratic 20% B for 2 min, followed by 20–50% B

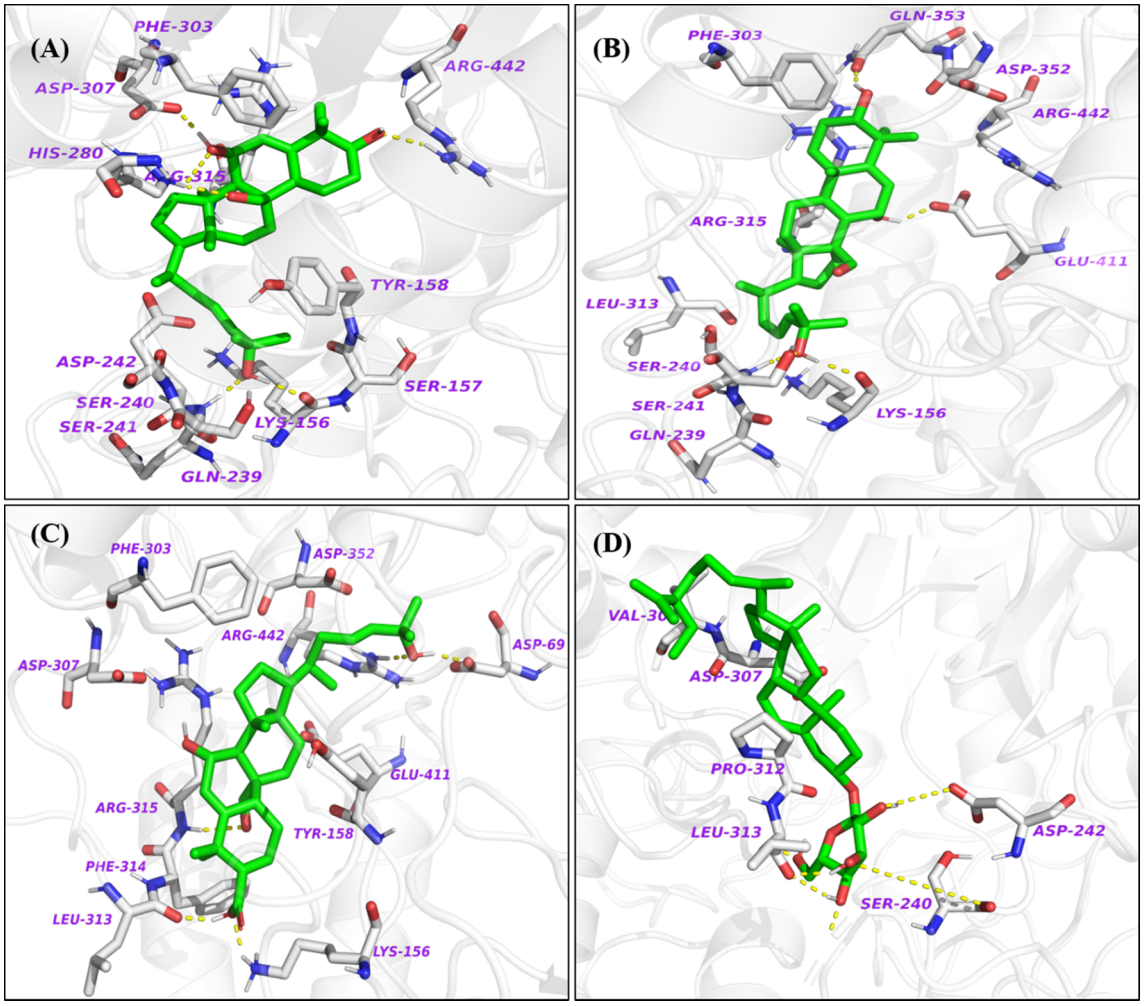

Fig. 5. The 3D ligand-protein interactions for (A). 3β,7β,25-trihydroxycucurbita-5,23(E)-dien-19-al, (B). charantal, (C). charantoside XI and (D). 25ξ-isopropenylchole-5, (6)-ene-3-O-β-D-glucopyranoside, in the binding pocket of α-glucosidase. The ligands in the 3D structure are shown in green and hydrogen bonds are shown in yellow. (For interpretation of the references to colour in this figure legend, the reader is referred to the web version of this article.)

(2–6 min), 50–90% B (7–10 min), and 90–95% B (11–18 min) followed by isocratic 95% B up to 23 min and returned to 20% B (24–26 min). The column was equilibrated for 2 min before the next injection. Flash chromatography system Teledyne ISCO CombiFlash Rf 4x system equipped with a fiber optic spectrometer, a UV–vis (λ200–700 nm) detector, was used for the purification. UPLC-HRESIMS were acquired using a maXis impact mass spectrometer (Bruker Daltonics, Billerica, MA) coupled to a 1290 Agilent LC (Agilent, Santa Clara, CA) using a quadrupole time of flight mass detector equipped with an electrospray ionization interface controlled by Bruker software (Bruker Compass DataAnalysis Version 4.2). The identification of the compounds was carried out using a Zorbax rapid resolution high definition eclipse plus C_{18} column (1.8 μm, 50 × 2.1 mm) (Agilent, Santa Clara, USA) at 65 °C with a flow rate of 0.5 mL/min using a binary mobile phase consisting of (A) 0.1% formic acid in water and (B) 0.1% formic acid in acetonitrile. The method was set for 16 min using 100–60% of A (0–8 min), 60–10% of A (8–13 min), and 10–100% of A (13–16 min). Samples were monitored at 210 and 280 nm. The NMR spectra 1D (^{1}H; ^{13}C and DEPT 135) and 2D NMR spectra were recorded with a JEOL spectrometer (USA, Inc., Peabody, MA) at 25 °C, operating at 400 MHz (^{1}H) and 100 MHz (^{13}C) using standard JEOL pulse programs. Samples were dissolved based on their solubility in methanol-d_4, pyridine-d_5, and $CDCl_3$.

4.3. Extraction

Fresh fruits of Chinese bitter melon (136 kg) were purchased from a local BCS Food Market. (College Station, TX) in October 2015. Fruits were chopped into small pieces, then the seed and fruit parts were separated and air dried. Dried samples of Chinese bitter melon were blended using a Vita-prep™ blender to 40–60 mesh size powder (Vita-Mix Corporation, Cleveland, OH). Total fruit powder (5.6 kg) was defatted using *n*-hexane and ethyl acetate using a Soxhlet apparatus at 60–70 °C for 32 h. Extracts were concentrated under reduced pressure using rotary evaporator (Buchi, New Castle, DE), freeze-dried and stored at −80 °C for further use. The EtOAc extract of 33.8 g (dry weight) was used for further experiments.

4.3.1. Fractionation of the crude ethyl acetate extract

The ethyl acetate crude (EtOAc) extract (33.8 g) was impregnated with 40 g of silica gel and chromatographed over silica gel (2.5 kg silica-gel 60 Å 40–63 μm) column chromatography. Initially, the column was eluted with *n*-hexane, *n*-hexane/EtOAc (95:5, 90:10, 85:15, 80:20, 60:40, 50:50, 40:60, 25:75, and 0:100 v/v) and a similar step gradient with EtOAc/acetone, acetone/MeOH and finally with MeOH to give 97 fractions of 300 mL each (Chromatography 1). Fractions were concentrated under reduced pressure using a rotary evaporator and pooled

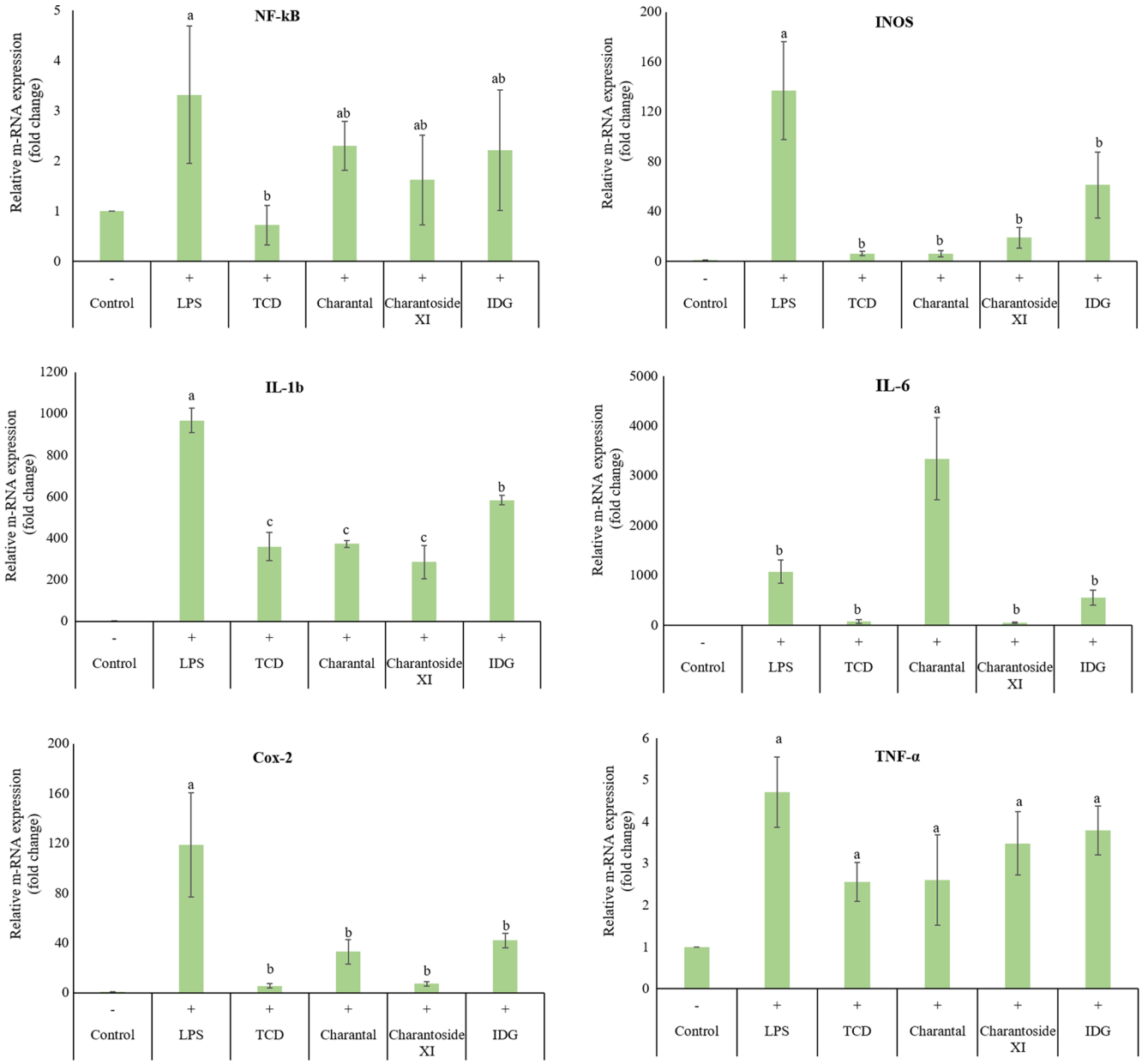

Fig. 6. Effect of purified compounds on m-RNA expression of *NF-κB*, *iNOS*, *IL-1β*, *IL-6*, Cox-*2* and TNF-*α* in LPS induced murine macrophage RAW 264.7 cells. Data are expressed as mean ± SD for (n = 9) and analyzed by one-way ANOVA. Identical letters within the same panel are not significantly different at $p \leq 0.001$ compared to LPS treatment group. Abbreviations TCD and IDG denotes 3β,7β,25-trihydroxycucurbita-5,23(E)-dien-19-al and 25ξ-isopropenylchole-5,(6)-ene-3-O-β-D-glucopyranoside, respectively.

based on TLC chromatographic profile. The schematic flow diagram for fractionation of EtOAc extract of Chinese bitter melon is shown in Fig. 7.

4.3.2. Purification

Fraction 20 (600 mg) from chromatography 1 was impregnated with 200 mg silica gel and air-dried in a hood. The air-dried sample was homogenized using a pestle and mortar. Next, the sample was subjected to flash chromatography in a 120 g silica gel cartridge, at 60 mL/min over 60 min, eluted using a gradient program with *n*-hexane and EtOAc from 100 to 0% with increasing polarity of eluents. In total, 210 fractions (15 mL each) were collected, and fractions were pooled based on silica gel TLC profiles to give subfractions 1–17. Subfractions 13 and 16 were crystallized in a test tube to yield compound **1** (15 mg), and fraction 16 yielded compound **2** (9 mg). Similarly, pools 25–30 of 1738 mg from chromatography 1 were subjected to flash chromatography using RP-Cosmosil 140 C_{18} column of 43 g using H_2O:MeOH (100–0%, 60 mL/min flow rate) linear gradient to afford 82 fractions, 1230 mL (82 × 15 mL each). Collected fractions were pooled based on HPLC retention time. Fractions 16–23, RT 14.2 min, H_2O:MeOH (15:85) were pooled to yield compound **3** (24.4 mg). Similarly, fractions 35–40 (1263 mg) from chromatography 1 were subjected to flash chromatography in a 120 g silica gel cartridge with a 90-min gradient program, flow rate of 85 mL/min of solvent A1 (ethyl acetate):B1 (acetone) gradient elution of 100–0% to give 113 fractions of 15 mL each. Fractions (84–92) (EtOAc:acetone 7:3) yielded compound **4** (24.9 mg).

4.4. Inhibition of α-amylase assay

α-Amylase inhibitory activity was determined using a published protocol with minor modifications [41]. All four compounds were

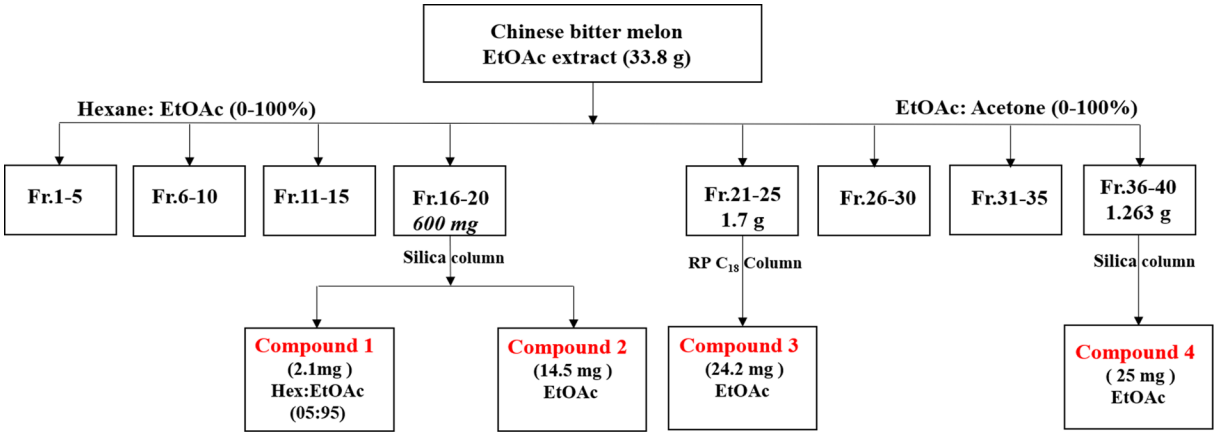

Fig. 7. Schematic flow diagram for purification of four compounds using column chromatography of Chinese bitter melon extract.

prepared to 10 mM in 500 µL DMSO and used for the inhibition of α-amylase assay. Two concentrations of 10 and 20 µL (equivalent to 0.43 and 0.86 mM) of all purified compounds were used for the assay, which was conducted in triplicate. The acarbose (10 and 20 µL equivalent to 0.067 and 0.13 mM) was used as a positive control. The absorbance was measured at 540 nm in a KC-4 microplate reader (BioTek Instruments, Inc., Winooski, VT) and % inhibition was calculated according to the published method.

4.5. Inhibition of α-glucosidase assay

The α-Glucosidase activity of purified compounds was determined according to the method with slight modifications, using α-glucosidase from *Saccharomyces cerevisiae* [42]. Acarbose was used as a standard in this experiment. The α-glucosidase activity was determined by measuring the yellow-colored para-nitrophenol released from pNPG at 405 nm. The absorbance was measured at 405 nm in a KC-4 microplate reader (BioTek Instruments, Inc., Winooski, VT, USA). Percentage inhibition was calculated as % Inhibition = $(Abs_{control} - Abs_{test}) \times 100/Abs_{control}$.

4.6. In silico molecular docking of purified compounds against α-amylase and α-glucosidases

Mode of inhibition of compounds **1–4** on the Porcine Pancreatic α-amylase (PPA) and isomaltase enzymes was further assessed by molecular docking analysis.

4.6.1. Preparation of protein structure

The 3-D coordinates of the crystal structures of proteins were downloaded from the RCSB protein data bank (PDB, http://www.rcsb.org/pdb) in PDB format. Porcine Pancreatic α-amylase complexed with acarbose (PDB ID: 1OSE) was downloaded from the PDB. The complexed acarbose was removed using Biovia Discovery studio 4.5 (DS 4.5, Dassault Systems BIOVIA, Discovery Studio Modeling Environment, Release 4.5, San Diego. 2015). Similarly, for α-glucosidase, the crystal structure (PDB ID: 3A4A) of isomaltase from *S. cerevisiae* was downloaded from the PDB. Later, both proteins were prepared by removing all water molecules, and a CHARMm force field was applied using the Receptor-Ligand interactions tool in DS.

Further, binding of acarbose to 1OSE and active residues of crystal structure of isomaltase were identified using the Computer Atlas of Topography of Proteins (CASTp), a program for identifying and characterizing active protein sites, binding sites, and functional residues located on the protein surface. The discovery studio tool was used to convert these files into the PDB format. Two-dimensional structures of purified compounds were drawn using ChemDraw tool (PerkinElmer Informatics, 2016) and saved as a molecular format file (MDL MOL format). The "Prepare ligand" protocol of DS 4.5 was used to prepare the ligands which remove duplicate structures, standardizes the charges of common groups, calculates the ions and ionization of the ligand's functional groups, 2D-3D conversion, verifying and optimizing the structures, and other tasks established by user-defined parameters. All the ligands were typed with the CHARMM36 force field using DS 4.5.

4.6.2. Molecular docking using Autodock 4.2

The four ligands were docked with α-amylase and α-glucosidase using the Lamarckian genetic algorithm (LGA) provided by the AutoDock Program (ADT, version: 1.5.6) version 4.2. Polar hydrogens were added to the receptor, Kollman charges were assigned, and solvation parameters were added with the "Addsol" option in AutoDock. Further, charges of the Gasteiger type were assigned. The internal degree of freedom and torsion were defined using the "Ligand Torsions" menu option of AutoDock. The grid maps representing the protein were calculated using the "AutoGrid" option. The protein was centered on the geometric center prior to docking, and the dimensions of the cubic grid box were set to 126 Å of x, y, and z with a spacing of 0.375 Å for the both proteins. Blind Docking was carried over the whole receptors (i.e., 1OSE and 3A4A) using Genetic Algorithm. The best ligand-receptor structure from the docked structures was chosen based on the lowest energy and minimal solvent accessibility of the ligand. The 2D visualization of ligand interactions with the protein domain was analyzed using DS 4.5, and PyMOL molecular graphics system (PyMOL Molecular Graphics System, San Carlos, CA, USA) was used to better visualize the 3D interactions between ligands and receptors.

4.7. Cell culture and maintenance

The RAW 264.7 mouse monocyte-macrophage cell line was procured from American Type Culture Collection (ATCC, USA) and cultured in RPMI 1640 medium supplemented with 10% (*v/v*) fetal bovine serum and antibiotics (100 U/mL penicillin and 100 µg/mL streptomycin). Cells were incubated at 37 °C in a humidified incubator with 5% CO_2. The media was changed every 48 h and cells that reached 80% confluence were used for further experiments.

4.7.1. RNA isolation and quantitative real-time polymerase chain reaction (qRT-PCR)

RAW 264.7 cells were seeded into 6-well plates at a density of 5.0×10^5 cells/well. Cells were incubated at 37 °C and 5% CO_2 for 24 h. Following incubation, the cells were treated with 25 µM of purified compounds (**1–4**) for 1 h. After 1 h, LPS (1 µg/mL) was added to specified wells, and the cells were incubated for an additional 18 h. Following the incubation period, total RNA was extracted using the

Aurum Total RNA Mini Kit. RNA concentrations were determined using a Nanodrop Spectrophotometer (Thermo Scientific NanoDrop Products). Purified RNA from cell lysate was used to synthesize cDNA according to the manufacturer's manual (iScript cDNA Synthesis Kit, Bio-Rad). Real-time PCR was performed on a Bio-Rad using the SYBR Green PCR Master Mix, according to the protocol provided by the manufacturer and relative expression was compared and normalized to the expression of *GAPDH* in the same sample. The primers' sequences are available on request. The m-RNA expression levels were analyzed by RT-PCR after 18 h of LPS treatment. Nontreated cells were used as negative control, and LPS-stimulated cells were used as a positive control.

5. Statistical analysis

Statistical analysis was performed using JMP Pro14 (SAS, NC, U.S.A.) statistical software. All data were expressed as mean ± SD. All statistical comparison compared through one-way analysis of variance (ANOVA), using Tukey's HSD post hoc test ($p \leq 0.01$, $n = 3$).

Conflicts of interest

The authors declare no conflict of interest.

Acknowledgments

This study was supported by the United States Department of Agriculture-NIFA-SCRI-2017-51181-26834 through the National Center of Excellence for Melon at the Vegetable and Fruit Improvement Center of Texas A&M University.

Appendix A. Supplementary material

Supplementary data to this article can be found online at https://doi.org/10.1016/j.bioorg.2019.02.040.

References

[1] L. Flores-Bocanegra, A. Pérez-Vásquez, M. Torres-Piedra, R. Bye, E. Linares, R. Mata, α-Glucosidase inhibitors from *Vauquelinia corymbosa*, Molecules 20 (2015) 15330–15342.
[2] P. Rathinavelusamy, P.M. Mazumder, D. Sasmal, V. Jayaprakash, Evaluation of *in silico, in vitro* α-amylase inhibition potential and antidiabetic activity of *Pterospermum acerifolium* bark, Pharm. Biol. 52 (2014) 199–207.
[3] M. Taha, S.A.A. Shah, M. Afifi, S. Imran, S. Sultan, F. Rahim, K.M. Khan, Synthesis, α-glucosidase inhibition and molecular docking study of coumarin based derivatives, Bioorg. Chem. 77 (2018) 586–592.
[4] A. Farooq, L. Shahazadi, M. Bajda, N. Ullah, A. Rauf, S.A. Shahzad, A.F. Khan, M. Ashraf, M. Yar, Organocatalyzed novel synthetic methodology for highly functionalized piperidines as potent α-glucosidase inhibitors, Arch. Pharm. 349 (2016) 724–732.
[5] K.-T. Kim, L.-E. Rioux, S.L. Turgeon, Alpha-amylase and alpha-glucosidase inhibition is differentially modulated by fucoidan obtained from *Fucus vesiculosus* and *Ascophyllum nodosum*, Phytochemistry 98 (2014) 27–33.
[6] J. Grover, S. Yadav, Pharmacological actions and potential uses of *Momordica charantia*: a review, J. Ethnopharmacol. 93 (2004) 123–132.
[7] J.L. Perez, G.K. Jayaprakasha, K. Crosby, B.S. Patil, Evaluation of bitter melon (*Momordica charantia*) cultivars grown in Texas and levels of various phytonutrients, J. Sci. Food Agric. 99 (2019) 379–390.
[8] C.-I. Chang, C.-R. Chen, Y.-W. Liao, H.-L. Cheng, Y.-C. Chen, C.-H. Chou, Cucurbitane-type triterpenoids from the stems of *Momordica charantia*, J. Nat. Prod. 71 (2008) 1327–1330.
[9] J. Zhang, Y. Huang, T. Kikuchi, H. Tokuda, N. Suzuki, K.i. Inafuku, M. Miura, S. Motohashi, T. Suzuki, T. Akihisa, Cucurbitane triterpenoids from the leaves of *Momordica charantia*, and their cancer chemopreventive effects and cytotoxicities, Chem. Biodiversity 9 (2012) 428–440.
[10] J.L. Perez, G.K. Jayaprakasha, B.S. Patil, Separation and identification of cucurbitane-type triterpenoids from bitter melon, ACS Symp. Ser. 1185 (2014) 51–78.
[11] X. Wang, W. Sun, J. Cao, H. Qu, X. Bi, Y. Zhao, Structures of new triterpenoids and cytotoxicity activities of the isolated major compounds from the fruit of *Momordica charantia* L. J. Agric. Food Chem. 60 (2012) 3927–3933.
[12] T. Akihisa, N. Higo, H. Tokuda, M. Ukiya, H. Akazawa, Y. Tochigi, Y. Kimura, T. Suzuki, H. Nishino, Cucurbitane-type triterpenoids from the fruits of *Momordica charantia* and their cancer chemopreventive effects, J. Nat. Prod. 70 (2007) 1233–1239.
[13] M.-J. Tan, J.-M. Ye, N. Turner, C. Hohnen-Behrens, C.-Q. Ke, C.-P. Tang, T. Chen, H.-C. Weiss, E.-R. Gesing, A. Rowland, Antidiabetic activities of triterpenoids isolated from bitter melon associated with activation of the AMPK pathway, Chem. Biol. 15 (2008) 263–273.
[14] H.-L. Cheng, H.-K. Huang, C.-I. Chang, C.-P. Tsai, C.-H. Chou, A cell-based screening identifies compounds from the stem of *Momordica charantia* that overcome insulin resistance and activate AMP-activated protein kinase, J. Agric. Food Chem. 56 (2008) 6835–6843.
[15] J. Efird, Y. Choi, S. Davies, S. Mehra, E. Anderson, L. Katunga, Potential for improved glycemic control with dietary *Momordica charantia* in patients with insulin resistance and pre-diabetes, Int. J. Environ. Res. Public Health 11 (2014) 2328–2345.
[16] B. Joseph, D. Jini, Antidiabetic effects of *Momordica charantia* (bitter melon) and its medicinal potency, Asian Pac. J. Trop. Dis. 3 (2013) 93–102.
[17] T.A. Pearson, G.A. Mensah, R.W. Alexander, J.L. Anderson, R.O. Cannon III, M. Criqui, Y.Y. Fadl, S.P. Fortmann, Y. Hong, G.L. Myers, Markers of inflammation and cardiovascular disease: application to clinical and public health practice: a statement for healthcare professionals from the Centers for Disease Control and Prevention and the American Heart Association, Circulation 107 (2003) 499–511.
[18] M. Shahinozzaman, N. Taira, T. Ishii, M. Halim, M. Hossain, S. Tawata, Anti-Inflammatory, anti-diabetic, and anti-Alzheimer's effects of prenylated flavonoids from Okinawa propolis: an investigation by experimental and computational studies, Molecules 23 (2018) 2479.
[19] S. Himaya, B. Ryu, Z.-J. Qian, S.-K. Kim, Paeonol from *Hippocampus kuda* Bleeler suppressed the neuro-inflammatory responses *in vitro* via NF-κB and MAPK signaling pathways, Toxicol. In Vitro 26 (2012) 878–887.
[20] C.P. Domingueti, L.M.S.A. Dusse, M. das Graças Carvalho, L.P. de Sousa, K.B. Gomes, A.P. Fernandes, Diabetes mellitus: the linkage between oxidative stress, inflammation, hypercoagulability and vascular complications, J. Diab. Complicat. 30 (2016) 738–745.
[21] C.-C. Liaw, H.-C. Huang, P.-C. Hsiao, L.-J. Zhang, Z.-H. Lin, S.-Y. Hwang, F.-L. Hsu, Y.-H. Kuo, 5β,19-epoxycucurbitane triterpenoids from *Momordica charantia* and their anti-inflammatory and cytotoxic activity, Planta Med. 81 (2015) 62–70.
[22] T.-H. Tsai, W.-C. Huang, H.-T. Ying, Y.-H. Kuo, C.-C. Shen, Y.-K. Lin, P.-J. Tsai, Wild bitter melon leaf extract inhibits *Porphyromonas gingivalis*-induced inflammation: identification of active compounds through bioassay-guided isolation, Molecules 21 (2016) 454.
[23] M.O. Fatope, Y. Takeda, H. Yamashita, H. Okabe, T. Yamauchi, New cucurbitane triterpenoids from *Momordica charantia*, J. Nat. Prod. 53 (1990) 1491–1497.
[24] B.G. Panlilio, A.P.G. Macabeo, M. Knorn, P. Kohls, P. Richomme, S.F. Kouam, D. Gehle, K. Krohn, S.G. Franzblau, Q. Zhang, A lanostane aldehyde from *Momordica charantia*, Phytochem. Lett. 5 (2012) 682–684.
[25] L. Peng, L. Jian-Feng, K. Li-Ping, Y. He-Shui, L.-J. Zhang, S. Xin-Bo, M. Bai-Ping, A new C30 sterol glycoside from the fresh fruits of *Momordica charantia*, Chin. J. Nat. Med. 2 (2012) 88–91.
[26] J. Chen, R. Tian, M. Qiu, L. Lu, Y. Zheng, Z. Zhang, Trinorcucurbitane and cucurbitane triterpenoids from the roots of *Momordica charantia*, Phytochemistry 69 (2008) 1043–1048.
[27] G.-T. Zhao, J.-Q. Liu, Y.-Y. Deng, H.-Z. Li, J.-C. Chen, Z.-R. Zhang, L. Zhou, M.-H. Qiu, Cucurbitane-type triterpenoids from the stems and leaves of *Momordica charantia*, Fitoterapia 95 (2014) 75–82.
[28] L. Harinantenaina, M. Tanaka, S. Takaoka, M. Oda, O. Mogami, M. Uchida, Y. Asakawa, *Momordica charantia* constituents and antidiabetic screening of the isolated major compounds, Chem. Pharm. Bull. 54 (2006) 1017–1021.
[29] M. Taha, S. Imran, F. Rahim, A. Wadood, K.M. Khan, Oxindole based oxadiazole hybrid analogs: novel α-glucosidase inhibitors, Bioorg. Chem. 76 (2018) 273–280.
[30] G.D. Brayer, Y. Luo, S.G. Withers, The structure of human pancreatic α-amylase at 1.8 Å resolution and comparisons with related enzymes, Protein Sci. 4 (1995) 1730–1742.
[31] A.T. Bale, K.M. Khan, U. Salar, S. Chigurupati, T. Fasina, F. Ali, A. Wadood, M. Taha, S.S. Nanda, M. Ghufran, Chalcones and bis-chalcones: as potential α-amylase inhibitors; synthesis, *in vitro* screening, and molecular modelling studies, Bioorg. Chem. 79 (2018) 179–189.
[32] M. Qian, R. Haser, G. Buisson, E. Duee, F. Payan, The active center of a mammalian. alpha.-amylase. Structure of the complex of a Pancreatic alpha.-amylase with a carbohydrate inhibitor refined to 2.2A. Resolution, Biochemistry 33 (1994) 6284–6294.
[33] X. Sui, Y. Zhang, W. Zhou, *In vitro* and *in silico* studies of the inhibition activity of anthocyanins against porcine pancreatic α-amylase, J. Funct. Foods 21 (2016) 50–57.
[34] A.A. Adegboye, K.M. Khan, U. Salar, S.A. Aboaba, S. Chigurupati, I. Fatima, M. Taha, A. Wadood, J.I. Mohammad, H. Khan, 2-Aryl benzimidazoles: synthesis, In vitro α-amylase inhibitory activity, and molecular docking study, Eur. J. Med. Chem. 150 (2018) 248–260.
[35] H. Sun, D. Wang, X. Song, Y. Zhang, W. Ding, X. Peng, X. Zhang, Y. Li, Y. Ma, R. Wang, Natural prenylchalconaringenins and prenylnaringenins as antidiabetic agents: α-glucosidase and α-amylase inhibition and *in vivo* antihyperglycemic and antihyperlipidemic effects, J. Agric. Food Chem. 65 (2017) 1574–1581.
[36] M.T. Javid, F. Rahim, M. Taha, H.U. Rehman, M. Nawaz, S. Imran, I. Uddin, A. Mosaddik, K.M. Khan, Synthesis, *in vitro* α-glucosidase inhibitory potential and molecular docking study of thiadiazole analogs, Bioorg. Chem. 78 (2018) 201–209.
[37] A.A. Alghasham, Cucurbitacins – a promising target for cancer therapy, Int. J. Health Sci. 7 (2013) 77.
[38] H. Sun, W.-S. Fang, W.-Z. Wang, C. Hu, Structure-activity relationships of oleanane- and ursane-type triterpenoids, Bot. Stud. 47 (2006) 339–368.

[39] T. Moses, K.K. Papadopoulou, A. Osbourn, Metabolic and functional diversity of saponins, biosynthetic intermediates and semi-synthetic derivatives, Crit. Rev. Biochem. Mol. Biol. 49 (2014) 439–462.
[40] L.-W. Qi, C.-Z. Wang, C.-S. Yuan, American ginseng: potential structure–function relationship in cancer chemoprevention, Biochem. Pharmacol. 80 (2010) 947–954.
[41] H. Shanmugam, P. Acharya, G.K. Jayaprakasha, B.S. Patil, Nanoformulation and characterization of nomilin with different poly (lactic-co-glycolic acid) resomers and surfactants for the enhanced inhibition of α-amylase and angiotensin-converting-enzyme, J. Funct. Foods 37 (2017) 564–573.
[42] G. Fu, W. Li, X. Huang, R. Zhang, K. Tian, S. Hou, Y. Li, Antioxidant and alpha-glucosidase inhibitory activities of isoflavonoids from the rhizomes of *Ficus tikoua* bur, Nat. Prod. Res. 32 (2018) 399–405.